Journal of Autonomous Intelligence (2024) Volume 7 Issue 5
doi: 10.32629/jai.v7i5.1630

ORIGINAL RESEARCH ARTICLE

Automated detection and classification of neurodegenerative diseases using time-frequency based methods and artificial neural network classifier

J. Prasanna[1,*], S. Thomas George[1], M. S. P. Subathra[2], C. Prajitha[3]

[1] *Department of Biomedical Engineering, Karunya Institute of Technology and Sciences, Coimbatore 641114, Tamil Nadu, India*

[2] *Department of Robotics Engineering, Karunya Institute of Technology and Sciences, Coimbatore 641114, Tamil Nadu, India*

[3] *Department of Electronics and Communication Engineering/Centre for Interdisciplinary Research, Karpagam Academy of Higher Education, Coimbatore 641021, India*

*** Corresponding author:** J. Prasanna, prasu1796@gmail.com

ABSTRACT

Background: Neurodegenerative diseases (NDDs) such as Huntington's disease (HD), amyotrophic lateral sclerosis (ALS), and Parkinson's disease (PD) are reflected in fluctuations in gait dynamics and affect motor activity. The classification of gait data using machine learning techniques can help physicians diagnose a neural disorder early when clinical symptoms are not yet visible. **Problems identified:** Because NDD can cause gait abnormalities, screening for NDD using a gait signal is a viable option. **Proposed work:** This study aimed to develop an automated system for differentiating NDDs from a healthy control (HC) group. This study used frequency and time-frequency-based techniques, namely Fast Walsh Hadamard Transform (FWHT) and Fourier synchrosqueezed transform (FSST), to analyze the gait time series. Statistical and entropy measures are computed to capture the non-linear characteristics in the gait fluctuating patterns while performing extended gait analysis. Furthermore, we investigated the impact of the proposed technique with different feature rankings to select optimum features from the time series gait dynamics data. **Research findings:** The efficient features have been computed for the classification where an artificial neural network (ANN) classifier is utilized to effectively classify gait abnormalities, which attains better performance in each classification task. The classification performance of the proposed study is compared with the traditional approach, where it outperforms with the highest classification accuracy.

Keywords: neurodegenerative disease; feature extraction; artificial neural network; classification

ARTICLE INFO

Received: 5 March 2024
Accepted: 29 March 2024
Available online: 23 May 2024

1. Introduction

Neurodegenerative diseases (NDDs) are disorders characterized by selective neuronal loss and distinguishable active participation of functional systems. Because the central nervous system regulates the flexion and extension motions of two lower limbs, the gait of a patient with a neurodegenerative disorder might become unusual due to motor neuron degradation. Thus, gait parameter evaluation is precious for gaining a greater comprehension of the processes underlying neurological conditions and the innovation of NDDs. Patients suffering from neurodegenerative diseases have a distinct gait pattern[1]. There are numerous NDDs, including Parkinson's disease (PD), Huntington's disease (HD), and amyotrophic lateral sclerosis (ALS). Worldwide, the estimated incidence of NDDs is

about 13.43 per 100,000 for PD, 5.70 per 100,000 for HD, and 2.7 per 100,000 for ALS[2]. Huntington's disease is a neurodegenerative condition that affects cognitive, motor, and psychiatric functions. Furthermore, ALS is a chronic and fatal form of motor neuron disease and the third most common NDD[3]. The disorders above are caused by structural proteins in various brain regions, leading to cell dysfunction or death, which causes abnormal movements[4]. ALS is characterized by progressive muscle atrophy, complexity with voluntary motor actions, and cognitive dysfunction due to damage to upper and lower motor neurons in the cerebral cortex, brain stem, and spinal cord[5].

Parkinson's disease is associated with abnormal endorphin neuron activity, which alters basal ganglia output[6]. The presence of neurological deficits, incurability, and the progressive nature of the illness are the prominent resemblances between PD, HD, and ALS, which may make a significant contribution to some motor symptom volatility. However, the initial motor symptoms of PD and HD are distinctive, so Parkinsonian signs manifest in many HD patients[7]. Still, with the progression of the disease, it is critical to distinguish between these disorders to identify specific NDD characteristics. Furthermore, an investigation of various aspects of movement damage in different NDDs based on behaviour for the same mobility task will aid in determining the findings[8]. Previous research has found that using Gait data resources results in promising NDD identification and assessment via gait recognition using time series data collected by chronoscopes and Inertial Measurement Unit (IMU)[9]. Researchers have focused on gait analysis in the last decade, notably time series of stride, stance, swing periods, vertical ground reaction force (VGRF), and foot pressure. Previous research has demonstrated that unique gait features can be classified using feature extraction methods and machine learning. Xia et al.[10] proposed a method for categorizing gait rhythm signals in NDD patients and healthy people. It describes how deterministic learning was used to identify healthy controls and patients with neurodegenerative diseases. However, gait recognition necessitates a wealth of fine-grained features because differences between gait styles are typically much more nuanced than those between standard action classifications. In the study of Zeng and Wang[11], different sensors are used to collect data that describes multi-modality gait characteristics to capture the subtle features without losing other key biomarkers. Research works of Poria et al.[12] examined diverse data collected from accelerometers, smartphones, or cameras for classification methods and found that it significantly improved performance over modality strategies. The VGRF assessment methods look for abnormal alterations to human foot speed by analyzing the force signals from each sensor under the left and right feet. In this regard, mobile or wearable health surveillance systems are small. So, for diagnostic applications, a portable sensor device is employed to measure kinematic and neurobiological function[13]. Therefore, many attempts have been made in this regard to distinguish all three groups, including ALS, PD, and HD patients, from healthy control (HC) subjects using various measures[14]. NDDs and healthy subjects have different stride time intervals, which show more minor scale adjustments in their feet. The force-sensing information in gait dynamics senses it. Gait images[15] depict the overall anatomy of a person's body, whereas acceleration and 3D skeleton data concentrate on the segments, sub of joints and the change in gait speeds. Variations in a series of stride intervals between time instants of consecutive ground contact events for either foot showcase subtle changes during the steady state of human walking.

Wu et al.[16] measured signal variations in PD patients' gait rhythm time-series data using entropy metrics. This study for assessing stride fluctuations in PD is used to compute the approximate Entropy, normalized symbolic Entropy, and signal turns count parameters. Another challenging factor for real-time detection techniques is execution time[17]. Liu et al.[18] and Yu et al.[19] used multi-scale approximate Entropy (MAE)[18] and symbolic Entropy[19] to analyze the ground reaction forces on both feet and compute the complexity of human gait. Liao et al.[20] applied the multi-resolution entropy analysis of stance time fluctuation to investigate the gait asymmetry. The derived phase synchronization and conditional entropy features from gait cycle patterns to distinguish them from healthy control (HC) gait patterns. After analyzing

the research articles, the entropy-based approaches paved a novelty for the proposed NDDs.

Time domain (TD) and time-dependent spectral features (PSDTD) were studied by Mengarelli et al.[21] to identify different forms of NDD. We analyzed stride-to-stride fluctuation data from various populations, including healthy controls (CN) and those with PD, HD, and AS. The study's findings show that NDD identification is accomplished using easily extracted and computationally light TD and PSDTD characteristics. These features may also be used to build computer-aided NDD detection systems for gait rhythm.

To categorize neurodegenerative disorders (NDDs) using the vGRF signal, Setiawan et al.[22] used a deep learning method in this research. Different force pattern variations compared to healthy control (HC) may be indicated by the irregularity of NDD vGRF signals induced by gait disorders. Early diagnosis of NDDs, effective treatment planning, and monitoring of illness progression are the primary goals of this study. The suggested identification technique successfully distinguishes between HC individuals' and neurodegenerative disease patients' walking patterns using a time-frequency spectrogram of a vGRF signal.

A new method for identifying Parkinson's disease (PD) using speech signals was suggested by Pankaj Warule et al.[23] and is based on the Chirplet transform (CT). After using CT to get the time-frequency matrix (TFM) of every audio recording, we used this information to extract features based on time-frequency entropy (TFE). According to the data, TFE traits may be utilized to distinguish between people with PD and healthy controls (HCs) since they capture the alterations in speech resulting from the disease. Using the PC-GITA database's vowels and words, we verify the usefulness of the suggested framework. The findings show that the suggested entropy characteristics based on CT may accurately diagnose PD from a person's speech.

A convolutional neural network (CNN) and a wavelet coherence spectrogram of gait synchronization were created by Setiawan et al.[24] to categorize neurodegenerative diseases (NDD) using gait force data. The primary goal of this study was to provide medical professionals with tools for NDD screening that would aid in early diagnosis, better treatment planning, and disease progression monitoring. The suggested algorithm for NDD detection uses a time-frequency spectrogram of gait force signals to distinguish between HC and NDD patients' gait patterns. It achieves an AUC value of 0.97, a sensitivity of 94.34%, a specificity of 96.08%, and an accuracy of 96.37% through 5-fold cross-validation.

The summarization of our proposed work is contributed below:

- The gait time series of four classes, PD, HD, ALS, and HC, were analyzed based on time-frequency approaches using FWHT and FSST.
- Statistical and Entropy-based features have been extracted from the decomposed coefficients of the FWHT and FSST.
- Feature ranking methods, namely *t*-test, Kulback Leibler Divergence (KLD), and Chernoff bound (CB), are utilized to select the best features to maximize the classification performance.
- The proposed technique attained the maximum accuracy using the ANN technique with 99.58% for PD vs. HC, 99.95% for HD vs. HC 100% ALS vs. HC using FWHT & 99.76% for PD vs. HC, 99.86% for HD vs. HC and 100% ALS vs. HC using FSST.

The rest of the paper is organized as follows. Section 2 presents the proposed framework and feature extraction and ranking techniques; the experimental results with the considered classification tasks are depicted in section 3; the conclusion of the proposed method and the future directions are given in section 4.

2. Methods and materials

2.1. Dataset used

Data sets for analysis and categorizing are derived from gait time series data in the neurodegenerative

database[25], accessible online in PhysioNet. The database contains 64 gait recordings from 16 healthy controls, 13 subjects with ALS, 20 with HD, and 15 with PD. The healthy control group consists of subjects aged 20–74, the ALS group of subjects aged 36–70, the HD group of subjects aged 29–71, and the PD group of subjects aged 44–80[26].

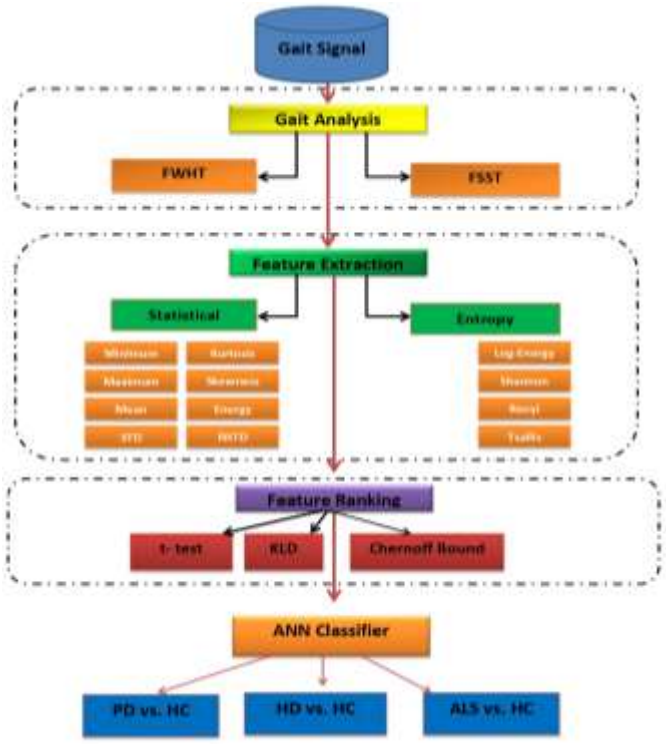

Figure 1. Functional block diagram of the proposed work.

Gait analysis is recorded from the gait signal as shown in **Figure 1**. Participants were instructed to walk at their comfortable pace for 5 min down a 77-meter-long passageway. Force-sensitive switches were placed in the subjects' shoes, and the output of these switches provided a force that was applied to the floor[27]. At a frequency of 300 Hz, a 12-bit built-in analog-to-digital converter was employed to collect data from the foot switches. The data included the temporal patterns of stride time (both left and right), stance time (both left and right), and swing time (both left and right). To mitigate initial fluctuations, the initial 20 s of recorded data were omitted, and a median filter was applied to eliminate data points that deviated significantly from the median value, as described in the work of Soubra[28]. The primary source of these outliers was the turning manoeuvres performed at the end of the hallway.

2.2. Fast Walsh Hadamard Transform

The Fast Walsh-Hadamard Transform (FWHT) is a highly effective algorithm employed for calculating the Walsh-Hadamard transform (WHT)[29]. The FWHT simplifies the computational complexity by using a divide-and-conquer strategy.

The FWHT procedure depicts the WHT through recursive steps[30] to fragment the sequence into smaller sub-sequences and merge their outcomes to achieve the ultimate transformation. It relies on the Walsh-Hadamard matrix[31], a square matrix with dimensions that are powers of 2.

Let's denote the input data sequence as $y(n)$, where n is the sequence length[32]. The FWHT equations can be defined as follows:

Base scenario: When n equals 1, the transformation equals the original input sequence.

Recursive scenario: In cases where *n* exceeds 1, you can compute the FWHT by splitting the sequence into two equal parts, applying the FWHT to each part, and subsequently merging the outcomes. The visual representation of the healthy signal from the Parkinson signal using FWHT is shown in **Figure 2**.

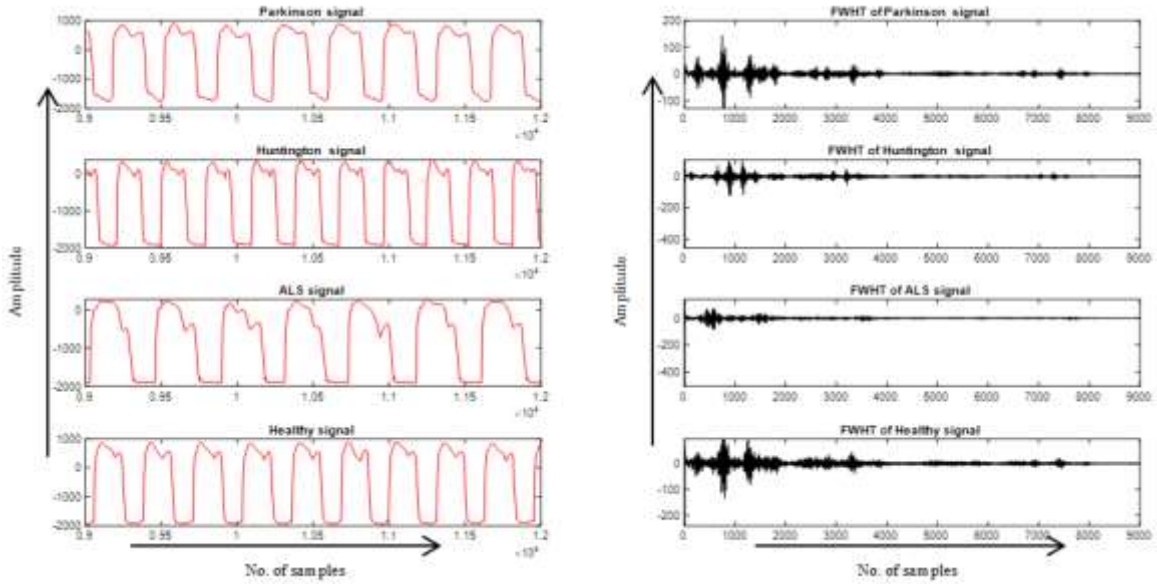

Figure 2. The visual representation of Hadamard coefficient decomposition using FWHT concerning NDDs.

The data samples of $y(n)$ and $n = 1,2,\ldots,N$ is given as below[33]:

$$XY_w(k) = \sum_{n=1}^{N} y(n) wf_n, k = 1,2,\ldots,N \tag{1}$$

In this context, where N represents the number of samples and wf_n denotes the Walsh function or Walsh matrix, which is determined by the following equation:

$$wf_n = \frac{1}{2^{\frac{n}{2}}} \begin{pmatrix} wf_{n-1} & wf_{n-1} \\ wf_{n-1} & -wf_{n-1} \end{pmatrix} \tag{2}$$

In a 1 × 1 matrix, the value of wf_0 is equal to 1. So that wf_1 and wf_2 can be written as:

$$wf_1 = \frac{1}{\sqrt{2}} \begin{bmatrix} 1 & 1 \\ 1 & -1 \end{bmatrix} \tag{3}$$

$$wf_2 = \frac{1}{2} \begin{bmatrix} 1 & 1 & 1 & 1 \\ 1 & -1 & 1 & -1 \\ 1 & 1 & -1 & -1 \\ 1 & -1 & -1 & 1 \end{bmatrix} \tag{4}$$

The Walsh function can alternatively be expressed as:

$$wf_n = \prod_{i=1}^{m} (-1)^{n_i k_{m-i}} \tag{5}$$

The FWHT results from multiplying a data sequence with a length of 1 × N by a Walsh matrix with dimensions of the $N \times N$ matrix.

2.3. Fourier synchrosqueezed transform

The Fourier Synchrosqueezed Transform (FSST) is a technique for analyzing time-frequency content that combines the strengths of the Fourier Transform (FT) with the synchrosqueezed transforms[34,35]. It is beneficial for studying signals with varying frequencies over time, including non-stationary signals or those exhibiting rapid changes in frequency[36].

Over the last decades, various approaches have been suggested to expand the principles of Fourier signal analysis to encompass non-stationary signals[37]. The FT of a signal, as expressed as

$$\hat{f}(q) = \int_{-\infty}^{\infty} f(t) e^{-i2\pi qt} \tag{6}$$

FT is suitable for stationary signals but is not well-suited for non-stationary signals. The Short-Time Fourier Transform (STFT) was introduced to address this limitation. STFT divides the signal into short intervals and applies the FT to each segment. In other words, STFT can be considered obtaining a local version of the FT using a sliding window (ω) approach.

$$S(q,t) = \int_{-\infty}^{\infty} x(\tau)\, \omega(\tau - t) e^{-i2\pi(\tau - t)d\tau} \tag{7}$$

Under the assumption of gradual changes in instantaneous frequencies, FSST offers a time-frequency representation of signals with multiple components. Therefore (q,t) , the synchrosqueezed transform decomposed the coefficients, which are defined as

$$(q,t) \rightarrow (q, \tilde{\varphi}(q,t)$$

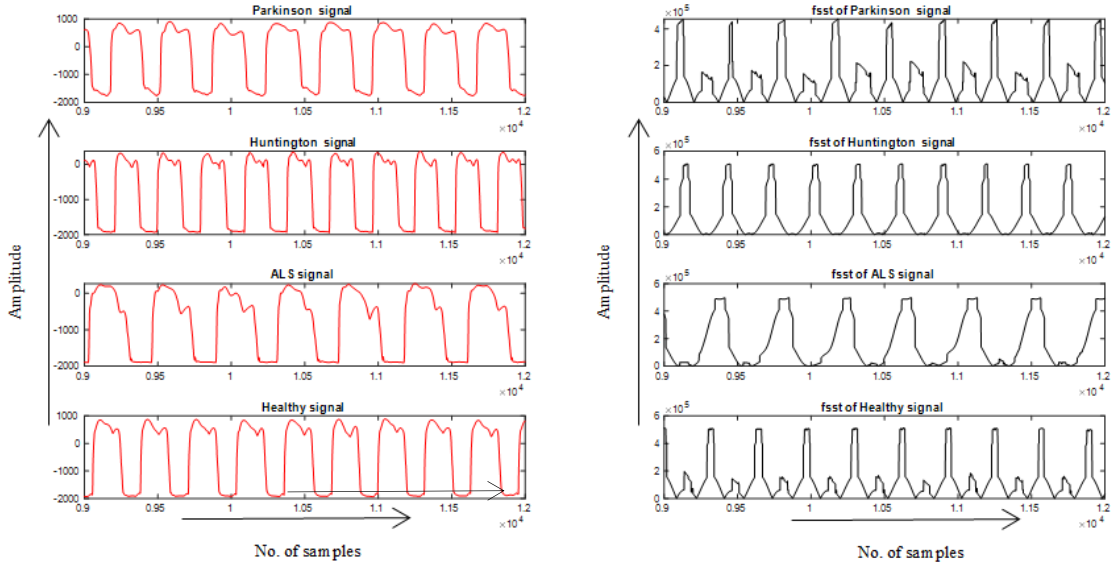

Figure 3. The visual representation of Fourier decomposition using FSST concerning NDDs.

where $\tilde{\varphi}$ corresponds to the instantaneous frequency of the time series expressed by

$$\tilde{\varphi}(q,t) = \frac{1}{2\pi} \frac{\partial(\arg S(q,t))}{\partial q} = Re\left(\frac{1}{2\pi i} \frac{1}{S(q,t)} \frac{\partial(S(q,t))}{\partial q}\right) \tag{8}$$

The visual representation of fourier decomposition using FSST is shown in **Figure 3**. The SST's second crucial component is "vertical reconstruction," provided that the window function is continuous and does not disappear at zero.

$$s(q) = \frac{1}{\omega(0)} \int_{-\infty}^{\infty} S(q,t) \mathrm{d}t \tag{9}$$

This allows for the definition of the FSST, which involves limiting the integration domain in the above equation to the interval determined by the expression, $\tilde{\varphi}(q,t) = \varphi$ can be written as

$$T(q,\varphi) = \frac{1}{\omega(0)} \int_{-\infty}^{\infty} S(q,t) \delta(\varphi - \tilde{\varphi}(q,t)) \mathrm{d}t \tag{10}$$

The FSST addresses certain constraints of the conventional FT[38], which offers a fixed time-frequency

resolution. The synchrosqueezing transform is employed on the FT spectrum within FSST to enhance the time-frequency precision of signal components. FSST furnishes a time-frequency portrayal of the signal that focuses the energy within the time-frequency domains where the signal components are situated. This enhances the ability to visualize and scrutinize the time-varying frequencies within the signal.

2.4. Feature extraction

Feature extraction involves extracting relevant information from raw data to create a concise representation. This process eliminates unnecessary data, improving the efficiency and accuracy of analysis[39]. Feature extraction was conducted on the transformed coefficients obtained from FWHT and FSST. This process yielded a total of twelve features, comprising eight statistical features (minimum, maximum, mean, STD, NSTD, kurtosis, skewness, and energy) and four entropy features (Log-Energy, Shannon, Renyi, and Tsallis). These features were computed from both the right and left foot gait series. The statistical features are calculated using **Table 1**.

Table 1. Mathematical expressions of the statistical features.

Features	Formula	Features	Formula
Minimum	M1 = Min(y_i)	Kurtosis	$\text{Kurt} = \frac{1}{n}\sum_{i=1}^{n}\left[\frac{(y_i-\bar{y})}{\sigma}\right]^4$
Maximum	M2 = Max(y_i)	Skewness	$\text{Skew} = \frac{1}{n}\sum_{i=1}^{n}\left[\frac{(y_i-\bar{y})}{\sigma}\right]^3$
Mean	$\mu = \sum_{1}^{n} y_i/n$	Energy	$\text{Energy} = \left[\sum_{i=1}^{n}\lvert y_i\rvert\right]^2$
STD	$\sigma = \sqrt{\sum(y_i-\mu)^2/n}$	NSTD	$\check{\sigma} = {}^{\sigma}/_{M2-M1}$

Entropy functions as a measure of uncertainty, quantifying the level of disorder in a signal[40]. Higher entropy values signify heightened uncertainty and greater chaos within the signal.

Log Energy entropy is specifically employed to assess the engagement of non-stationary signals. Its mathematical definition is as follows:

$$E_{\log} = \sum_{i=1}^{N} \log(y_i^2) \tag{11}$$

where N represents the signal y_i's total length and the signal's i-th sample.

Shannon's Entropy is a metric that quantifies related parameters that exhibit a linear relationship with the logarithm of the number of possible outcomes. It is a measure used to assess the dispersion of data and is primarily employed to evaluate the dynamic structure of a system. One notable advantage of Shannon's Entropy is its suitability for characterizing data that follows a normal distribution[41].

$$E_{\text{Shannon}} = -\sum_{i=1}^{N} y_i \log(y_i) \tag{12}$$

Rényi entropy is an extended version of Shannon entropy, and it finds application in computing the spectral complexity and non-linearity of a time series signal. It can be expressed as[42,43]

$$E_{\text{Renyi}} = \frac{1}{1-\delta}\log_2 \sum_{i=1}^{N} {y_i}^{\delta} \tag{13}$$

In equation (13), δ corresponds to spectral order; when $\delta = 2$, it establishes a lower limit for its smooth Entropy. In contrast, when $\delta = 1$, it is analogous to Shannon's Entropy and tends to yield a relatively low

amount of smooth Entropy.

Tsallis entropy is a valuable tool for characterizing the physical behaviour of various systems. It is particularly effective in describing systems that exhibit long-term memory effects, involve long-range interactions, or are subject to multifractal space-time constraints. In the context of EEG signal analysis, Tsallis coefficients derived from Tsallis entropy can be instrumental in distinguishing between different gait patterns, such as spikes, bursts, and continuous rhythms. It can be mathematically expressed as[44,45]

$$E_{\text{Tsallis}} = \frac{1 - \sum_{i=1}^{N} {y_i}^q}{q - 1} \tag{14}$$

2.5. Feature ranking

Ranking holds significant importance in the realm of information retrieval. Although there has been extensive research on algorithms for learning ranking models, the same cannot be said for feature selection despite its significance[46]. Many feature selection techniques designed for classification are adapted for ranking tasks. However, we contend that due to the pronounced distinctions between ranking and classification, creating distinct feature selection methods explicitly tailored for ranking is more advantageous. This study uses five different feature ranking methods to select the optimum features.

2.5.1. *t*-test

The *t*-test is a statistical method used to select the best features. Its primary objective is to ascertain whether a substantial disparity exists between the means of two groups or variables of data. Through the application of the *t*-test[47], one can discern which features hold the greatest relevance or impact when predicting the target variable. The *t*-test calculates a *p*-value to determine the statistical significance within a chosen confidence interval. If the *p*-value is less than 0.05 (with a 95% confidence interval), it signifies different means concerning the group; otherwise, a *p*-value greater than 0.05 suggests identical means of the two groups.

t-test that can defined by

$$T = \frac{(\overline{y_1} - \overline{y_2})}{\sqrt{\frac{{sv_1}^2}{n1} + \frac{{sv_2}^2}{n2}}} \tag{15}$$

where y_1, y_2 are the samples from two different groups, and sv_1 and sv_2 are the computed variance of the samples of two groups that can be written as

$$\overline{sv_i} = \frac{\sum_{j-1}^{N} (y_i - \overline{y_i})^2}{N - 1} \tag{16}$$

In the above equation $\overline{y_i}$ corresponds to the sample mean.

2.5.2. Kullback Leibler divergence (KLD)

Kullback-Leibler Divergence (KLD) is used to simplify the clutter of non-dominant hypotheses by combining them into one event. It's also commonly used to identify discrepancies between two classifiers, which calculate posterior class probabilities for decision-making. However, KLD treats all class probabilities equally and doesn't emphasize the dominant hypotheses, which are especially important in classification scenarios[48].

Considering two group samples, y_1, y_2 and class probabilities are P_j and Q_j.

The KLD of Q_j from P_j is expressed as

$$DK(P, Q) = \sum_{j} Q_j \log \frac{Q_j}{P_j} \tag{17}$$

2.5.3. Chernoff bound

Chernoff bound is also called Bhattacharya distance. The Chernoff bound describes how the tail distributions of sums of independent random variables decrease exponentially. Considering the two classes' y_p and y_q, the minimum attainable classification error can be written as[49]:

$$P_{\text{error}} \leq P(y_p)^s P(y_q)^{1-s} \int_{-\infty}^{\infty} P(x|y_p)^{1-s} \mathrm{d}x \equiv \epsilon_{CB} \tag{18}$$

ϵ_{CB} is called Chernoff bound. This minimum bound and special bound are computed concerning s. it can be given as

$$P_{\text{error}} \leq \epsilon_{CB} = \sqrt{P(y_p)P(y_q)} \int_{-\infty}^{\infty} \sqrt{P(x|y_p)P(x|y_q)\mathrm{d}x} \tag{19}$$

where $\epsilon_{CB} = \sqrt{P(y_p)P(y_q)}\exp(-B)$

$$B = \frac{1}{8}(\mu_p - \mu_q)^T \left(\frac{\epsilon_p + \epsilon_q}{2}\right)^2 (\mu_p - \mu_q) + \frac{1}{2}\ln\frac{|(\epsilon_p + \epsilon_q)/2|}{\sqrt{|\epsilon_p||\epsilon_q|}} \tag{20}$$

and $|.|$ denotes the determinant of the respective matrix, and B indicates the Bhattacharya distance.

2.6. Artificial neural network classifier

An artificial neural network (ANN) classifier is a machine learning model influenced by the organization and operation of biological neural networks. Its primary purpose is categorizing input data into predefined classes or categories. ANN classifiers comprise layers of interconnected artificial neurons called nodes or units. The initial layer is the input layer, which receives the input data. The final layer is the output layer, which is responsible for generating the classification outcome. Between these layers, one or more hidden layers may exist tasked with processing input data to identify pertinent features and formulate predictions.

The classification of ANN types depends on the arrangement of neurons (network topology) and the training method. In this study, a well-established ANN type was employed, characterized by a layered, feed-forward network topology and the back-propagation training algorithm. The term "feed-forward topology" indicates that in this ANN, neurons are interconnected in a way that avoids feedback loops.

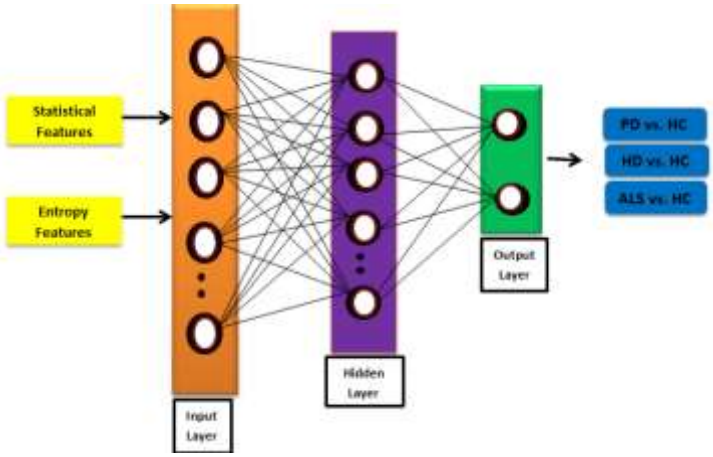

Figure 4. The Function Architecture of ANN classifier.

The Levenberg-Marquardt (LM) algorithm is an optimization technique applied to train artificial neural networks (ANNs). Its design is particularly well-suited for functions that take on the structure of a sum of squared errors, a common occurrence in the training of feed-forward neural networks. A total of 8 statistical

and 4 entropy features have been trained using the ANN classifier, 50 hidden neurons considered in the hidden layer, and the output layer consists of the different classes of NDDS and HC, as shown in **Figure 4**. In this paper, the consideration of the ANN classifier is given below:

- Total No. of layers: Five
- No. of hidden layers: Three
- No. of Input neurons: Equivalent to the size of the features
- No. of hidden neurons: Fifty
- No. of output neurons: Two
- The transfer function of the hidden layer: Hyperbolic tangent sigmoid
- The transfer function of the output layer: SoftMax
- Training function of the network: Levenberg-Marquardt (LM) algorithm
- Number of epochs: 100
- Performance function: Mean squared error

The classification performance is computed for individual HC, PD, HD & ALS subjects based on the classification results such as classification accuracy, sensitivity, specificity, positive predictive value and negative predictive value that are given by following formulas:

$$\text{Classification accuracy (AC)} = \frac{\text{True}(+) + \text{True}(-)}{\text{True}(+) + \text{True}(-) + \text{False}(+) + \text{False}(-)} \times 100 \tag{21}$$

$$\text{Sensitivity (SE)} = \frac{\text{True}(+)}{\text{True}(+) + \text{False}(-)} \times 100 \tag{22}$$

$$\text{Specificity (SP)} = \frac{\text{True}(-)}{\text{True}(-) + \text{False}(+)} \times 100 \tag{23}$$

$$\text{Positive predictive value (PPV)} = \frac{\text{True}(+)}{\text{True}(+) + \text{False}(+)} \times 100 \tag{24}$$

$$\text{Negative Predictive Value (NPV)} = \frac{\text{True}(-)}{\text{True}(-) + \text{False}(-)} \times 100 \tag{25}$$

where True(+) indicates True positive, True(−) refers to True negative, False(+) corresponds to False positive and False(−) implies False negative.

3. Experimental results and discussion

This study presents a publicly available dataset on gait dynamics related to neurodegenerative diseases to identify gait impairments in affected individuals. The dataset includes a total of 64 records from individuals with NDD, categorized as follows: 15 records from PD patients aged between 44–80 years, 20 records from HD patients aged between 29–71 years, 13 records from ALS patients aged between 36–70 years, and 16 records from healthy control subjects aged between 20–74 years. Each recording comprises a five-minute-long time series of gait signals collected using force-sensitive resistors placed under the patient's foot and sampled at a rate of 300 Hz. The dataset contains gait signals of 90,000 samples each, recorded from the left and right foot of four different groups of individuals. We utilized two effective feature extraction methods to analyze these gait signals: the FWHT and FSST. These techniques allowed us to perform frequency domain and time-frequency domain analysis on the gait series, enabling the decomposition of the NDD gait signals. A set of features was extracted from the decomposed coefficients, including eight statistical features and four entropy features. The study involved the analysis of gait signals from various groups, removing a wide range of features using FWHT and FSST, resulting in a substantial feature set for classification consisting of 1024 statistical features and 512 entropy features. The features extracted were used as input data for an ANN classifier. The ANN was trained using the Levenberg-

Marquardt training algorithm and configured with a hidden layer containing 50 neurons. This architecture and training approach were employed to classify the gait data based on the extracted features. **Table 2** shows the PD vs. HC classification performance in view of individual features using FWHT and FSST.

Table 2. Classification performance of PD vs. HC using FWHT & FSST (Considering single features).

PD vs. HC	**Classification results using FWHT (%)**					**Classification results using FSST (%)**					**Classification results using FWHT- FSST (%)**				
Features	**AC**	**SE**	**SP**	**PPV**	**NPV**	**AC**	**SE**	**SP**	**PPV**	**NPV**	**AC**	**SE**	**SP**	**PPV**	**NPV**
Minimum	91.90	91.21	91.53	92.54	91.79	91.96	91.37	91	91.84	90.45	92.08	91.25	92.95	91.75	90.12
Maximum	91.68	91.41	92.70	91.37	91.79	91.08	90.12	93.6	92.34	92.45	92.95	91.75	92.58	91.32	91.87
Mean	92.12	91.33	91.75	90.12	92.79	92.95	89.87	91.37	91.33	91.75	92.34	91	92	91.96	91.87
STD	88.4	88.61	89.32	89.87	90.91	90	91.87	91.01	88.61	89.32	93.61	91.32	92.82	91.57	91.01
Kurtosis	91.59	91.57	91.96	91.87	91.16	88.61	89.32	92.82	91.57	91.96	93.37	90.35	92.12	92.37	92.82
Skewness	91.5	91.01	91.08	89.25	90.95	91.37	90	90.12	93.6	91.08	93.01	91.21	92.87	92.33	92.75
Energy	92.12	92.82	92.95	91.75	92.58	91.01	91.21	89.87	91.37	92.95	93.82	92.62	92.61	91.61	92.32
Nstd	91.84	90.45	90.34	91	90	92.82	92.62	88.61	92.34	92.45	92	91.87	92.01	91.57	91.96
Log-Energy	92.34	92.45	92.34	93.6	92.45	93.4	93.61	91.57	91.33	91.75	93.61	91.32	92.82	91.90	91.96
Shannon	91.57	91.96	91.87	91.37	90	91.59	91.57	91.01	91.37	91.79	92.37	90.36	90.12	92.68	91.08
Renyi	92.95	91.75	92.79	91.01	91.21	91.87	91.37	92.82	90.12	92.79	92.01	91.21	91.87	92.12	93.95
Tsallis	**93.34**	93	91	92.82	92.62	**92.58**	91.01	91.34	91	91.45	**94.31**	92.59	93.57	93.4	94

As illustrated in **Table 2**, the proposed technique performed better even with a single feature. The classification performance of PD vs. HC using FWHT attained the accuracy ranges between 88.4%–93.34%, sensitivity between 88.61%–92.82%, specificity between 89.32%–92.79%, positive predictive value between 89.87%–93.6%), and negative predictive value 90%–92.79%). Entropy features attained maximum accuracy compared to statistical features. Tsallis entropy outperforms with 93.34% classification accuracy for the classification of PD vs. HC using FWHT, whereas log energy features outperform with classification accuracy of 93.4% using FSST. **Table 3** demonstrates the classification result of HD vs. HC.

Table 3. Classification performance of HD vs. HC using FWHT & FSST (Considering single features).

HD vs. HC	**Classification results using FWHT (%)**					**Classification results using FSST (%)**					**Classification results using FWHT-FSST (%)**				
Features	**AC**	**SE**	**SP**	**PPV**	**NPV**	**AC**	**SE**	**SP**	**PPV**	**NPV**	**AC**	**SE**	**SP**	**PPV**	**NPV**
Minimum	92.82	91.57	91.96	91.33	91.75	91.59	91.57	92.58	91.01	90.58	91.28	91.37	93.10	91.96	91.08
Maximum	92.34	93.6	92.90	91.3	91	91.01	91.37	93.6	92.34	92.45	90.15	91.12	90.91	92.05	92.56
Mean	91.01	91.37	92	90.56	93.10	88.88	89.78	90.37	90.12	91.21	92.38	91.50	90.32	90.95	91.28
STD	92.82	90.12	89.32	89.87	90.91	91.01	91.08	89.25	91.61	90.32	92.57	91.01	91.96	91.79	90.15
Kurtosis	91.55	91.50	91.02	91.16	91.28	88.61	89.32	92.82	91.57	91.96	92.37	92.83	92.82	92	91.37
Skewness	91.5	91.01	91.08	90.12	90.15	91.33	91.89	91.67	91.45	92.05	92.01	92.87	91.01	91.96	90.12
Energy	92.23	92.83	92.56	92.34	92.38	91.87	91.01	88.61	89.32	90.95	93.58	92.32	92.4	92.05	91.01
Nstd	89.25	90.95	91.37	91.59	91.57	90.91	92.4	91.87	90.12	92.79	93	92.96	91.87	92.12	92.4
Log-Energy	91.53	92.54	91.79	91.59	91.57	93.61	91.57	93.61	91.33	91.75	92.56	92.34	92.38	90.91	92.4
Shannon	88.4	88.61	91.70	91.78	91.30	88.61	91.57	91.01	91.37	91.79	92.37	92.82	92.82	91.21	92.33
Renyi	91.59	91.57	93.61	91.57	91.21	92.33	91.37	92.82	91.32	92	92.56	92.34	92.67	93.62	92.58
Tsallis	94.24	93	93.58	93.45	93.62	94.58	94.01	95.34	94.06	94.45	95.89	93.67	92.12	92.15	92.36

For the classification of HD vs. HC, the Tsallis entropy feature attained maximum accuracy of 94.24% and 94.58% using FWHT and FSST, respectively is shown in **Table 4**. Skewness from statistical features and Tsallis entropy attained maximum accuracy using the FWHT & Energy feature from statistical, and Tsallis Entropy attained maximum accuracy compared to other features.

Table 4. Classification performance of ALS vs. HC using FWHT & FSST (Considering single features).

ALS vs. HC	**Classification results using FWHT (%)**					**Classification results using FSST (%)**					**Classification results using FWHT-FSST (%)**				
Features	**AC**	**SE**	**SP**	**PPV**	**NPV**	**AC**	**SE**	**SP**	**PPV**	**NPV**	**AC**	**SE**	**SP**	**PPV**	**NPV**
Minimum	91.50	91.76	91.70	91.76	91.24	91.30	91.70	91.90	92.26	92.60	91.56	91.32	91.84	91.40	90.79
Maximum	92.42	91.67	92.19	91.22	91.62	92.65	92	91.56	92.31	90.00	92.43	91.50	92.45	91.49	92.60
Mean	91.87	92.57	91.16	91.17	91.56	91.68	91.29	91.06	90.78	91.96	91.90	91.67	91.76	91.40	90.64
STD	91.24	91.03	91.46	91.46	91.02	90.74	90.55	91.92	90.79	91.21	92.67	91.58	92.23	91.53	92.69
Kurtosis	92.07	92.75	91.41	92.42	91.72	90.20	91.65	91.76	92.60	91.84	91.87	92.77	91.56	90.27	91.57
Skewness	92.79	92.71	91.86	92.86	91.71	91.77	91.84	91.70	92.70	91.84	91.65	92.90	91.45	91.39	91.34
Energy	92.83	91.48	91.20	91.21	92.45	92.75	92.03	91.47	92.56	91.01	91.19	92.19	91.23	90.20	91.45
Nstd	92.52	92.17	92.89	92.90	92.15	92.67	92.46	91.88	91.58	91.40	91.23	92.34	91.28	91.05	91.75
Log-Energy	94.31	94.08	94.54	94.54	94.07	93.42	93.71	93.13	92.45	93.66	93.54	93.07	93.42	93.78	93.13
Shannon	93.81	93.99	92.74	92.76	93.85	93.58	93.10	93.05	93.37	93.05	92.76	93.45	93.78	93.17	93.09
Renyi	94.54	94.45	94.86	94.87	94.20	94.25	94.73	94.77	94.82	94.70	94.87	94.20	94.25	94.73	94.77
Tsallis	94.54	94.34	94.00	93.06	94.01	94.53	94.87	94.79	94.83	94.86	95.06	94.01	94.53	94.87	94.79

In classifying individuals with ALS from HC, it's important to highlight that single features yielded the best performance compared to other classification tasks. Specifically, Tsallis entropy achieved the highest classification accuracy of 96.54% when using the FWHT method. Similarly, Tsallis entropy demonstrated strong performance with an accuracy of 94.53% when using the FSST method. These results indicate that Tsallis entropy, when applied to the gait signals processed with either FWHT or FSST, was highly effective in distinguishing between individuals with ALS and healthy controls, achieving a very high classification accuracy in both cases.

To improve the classification performance, we employ three feature ranking techniques to select the best features from the Hadamard coefficients, which help reduce dimensionality with maximum classification results.

Table 5 demonstrates i) the classification performance of all three classification tasks considering all statistical features (length of 1024), all entropy features (Length of 512) and combined statistical and Entropy (Length of 1536), ii) features selected by t-test ranking method which result in dimensionality reduction of features with the length of 128 statistical and 128 entropy measures in all the cases. Similarly, iii & iv are the classification performance of the three cases using KLD and CB, respectively.

Table 5. Classification performance of NDD using FWHT and feature ranking (*t*-test, KLD, CB).

FWHT		**PD vs. HC (%)**			**HD vs. HC (%)**			**ALS vs. HC (%)**		
		ST	**EN**	**ALL**	**ST**	**EN**	**ALL**	**ST**	**EN**	**ALL**
Without feature ranking	AC	94.75	96.03	**97.47**	94.90	94.26	**96.60**	94.71	95.34	**96.17**
	SE	94.67	96.46	97.88	94.29	95.31	96	94.83	94.82	95.62
	SP	94.42	95.71	96.13	94.06	95.78	96	94.47	94.31	95.06
	PPV	94.58	96.10	96.05	94.92	95.79	96.21	94.54	94.15	96.87
	NPV	94.25	96.73	96.77	94.76	94.60	96.84	94.69	94.61	95.60

Table 5. (*Continued*).

FWHT		PD vs. HC (%)			HD vs. HC (%)			ALS vs. HC (%)		
		ST	EN	ALL	ST	EN	ALL	ST	EN	ALL
t-test	AC	97.84	98.59	**99.09**	97.70	98.70	**99.84**	96.70	97.81	**99.81**
	SE	97.61	98.00	99.23	96.47	98.56	99.01	96.60	97.98	99.60
	SP	97.41	97.51	99.32	97.88	98.58	99.40	96.99	97.17	99.92
	PPV	97.76	97.79	99.73	98.13	98.45	99.66	96.77	97.33	99.07
	NPV	97.28	98.08	99.48	97.05	98.37	99.05	96.20	97.25	99.97
KLD	AC	98.91	98.39	**99.43**	97.77	98.82	**99.70**	96.42	98.13	**99.55**
	SE	97.44	98.81	99.07	97.79	98.83	98.86	96.70	98.65	99.00
	SP	98.25	98.71	99.80	97.13	98.14	99.69	96.46	98.66	99.95
	PPV	98.72	99	99.92	97.12	98.13	99.65	96.04	98.51	99.79
	NPV	97.20	98.39	99.01	97.70	98.70	99.84	96.29	98.29	99.93
CB	AC	98.15	98.17	**99.58**	98.71	98.13	**99.95**	98.39	98.51	**100**
	SE	98.55	98.83	99.27	98.10	99.05	99.37	97.20	98.62	99.34
	SP	98.79	99.36	99.21	98.73	98.77	99.82	97.03	98.18	99.16
	PPV	98.48	98.93	99.03	98.87	98.79	99.83	97.33	98.15	99.51
	NPV	98.92	99.15	99	99.69	98.13	99.14	97.42	98.54	99.95

Without features selection, the proposed framework (FWHT) attained a maximum accuracy of 97.47% for PD vs. HC, 96.60% for HD vs. HC and 96.17% for ALS vs. HC with all the statistical and Entropy features. Using the t-test, the classification performance improved to 99.09% PD vs. HC, 99.84% for HD vs. HC and 99.81% for ALS vs. HC. The same was evaluated using KLD, which attained the classification accuracy of 99.43% (PD vs. HC), 99.70% (HD vs. HC) and 99.55% (ALS vs. HC). Comparatively, CB feature ranking outperforms in all the classification cases with an accuracy of 99.58%, 99.95% and 100% for classification between PD vs. HC, HD vs. HC and ALS vs. HC—the comparative results of the classification scheme depicted in **Figure 5**.

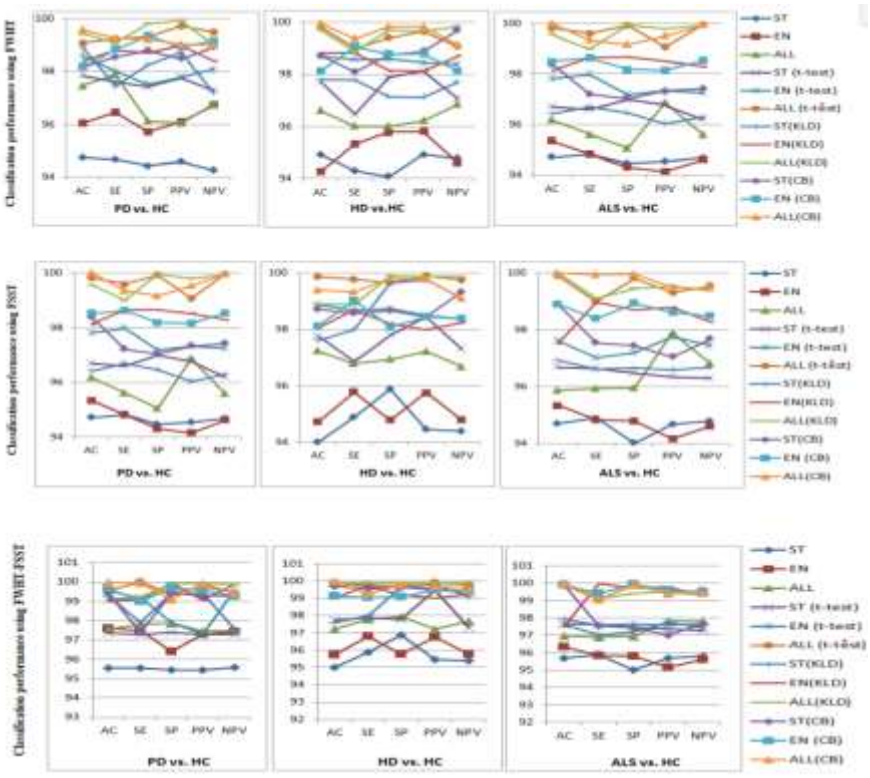

Figure 5. Comparative result of all the classification tasks using FWHT, FSST and Feature ranking techniques.

Table 6 shows the efficiency of the proposed work using FSST with feature raking techniques. The ANN classifier classified the statistical entropy features obtained from the Fourier decomposed coefficient. They attained the maximum accuracy of 97.98%, 97.23% and 95.87% for PD vs. HC, HD vs. HC and ALS vs. HC, respectively. The classification accuracy increased by 100% for ALS vs. HC using the CB feature ranking technique. **Figure 6** depicts the radar graph of the outcome, considering all features in every categorization method.

Table 6. Classification performance of NDD using FSST and feature raking (*t*-test, KLD, CB).

FSST		**PD vs. HC**			**HD vs. HC**			**ALS vs. HC**		
		ST	**EN**	**ALL**	**ST**	**EN**	**ALL**	**ST**	**EN**	**ALL**
Without feature ranking	AC	94.86	96.67	**97.98**	94	94.73	**97.23**	94.70	95.34	**95.87**
	SE	94.56	96.78	97.87	94.89	95.78	96.78	94.89	94.82	95.92
	SP	94.45	95.67	96.56	95.89	94.78	96.93	94	94.78	95.96
	PPV	94.43	96.56	96.85	94.45	95.76	97.21	94.67	94.15	97.88
	NPV	94.43	96.45	96.43	94.39	94.78	96.67	94.79	94.60	96.80
t-test	AC	97.67	98.39	**99.34**	97.76	98.87	**99.86**	96.67	97.63	**99.89**
	SE	97.23	98.89	99.98	96.86	98.68	99.78	96.63	97	99
	SP	97.45	97.92	99.24	97.78	98.73	99.65	96.46	97.19	99.80
	PPV	97.64	97.46	99.79	98.45	98.49	99.90	96.34	97.75	99.30
	NPV	97.02	98.81	99.40	97.29	98.38	99.76	96.29	97.43	99.54
KLD	AC	98.03	98.05	**99.34**	97.60	98.05	**98.90**	96.93	97.50	**100**
	SE	97.50	98.90	99	97.98	98.70	98.87	96.60	98.98	99.10
	SP	98.25	98.94	99.90	99.65	98.20	99.90	96.64	98.70	99.45
	PPV	98.65	98.05	99.90	99.76	98	99.87	96.59	98.78	99.54
	NPV	97.54	98.89	99.87	99.09	98.25	99.88	96.67	98.27	99.37
CB	AC	98.43	98.67	**99.76**	98.71	98.13	**99.40**	98.90	98.91	**100**
	SE	97.76	98.07	99.95	98.56	99.03	99.32	97.54	98.39	99.94
	SP	98	99.23	99.09	98.67	98.09	99.80	97.43	98.93	99.95
	PPV	98.56	98.09	98.90	98.45	98.45	99.78	97.03	98.60	99.48
	NPV	98.67	99.22	98.45	99.34	98.38	99.07	97.67	98.48	99.45

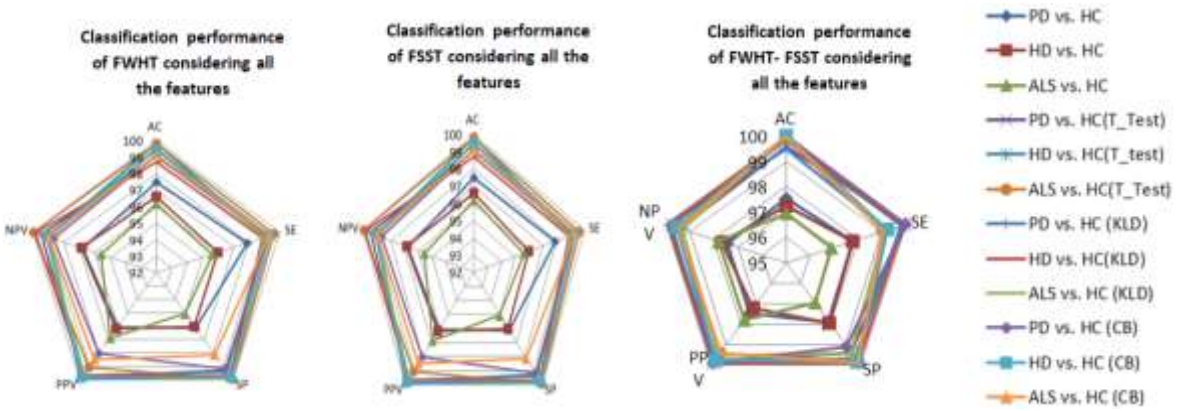

Figure 6. The overall classification performance of the proposed framework.

Table 7. Classification performance of NDD using FWHT-FSST and feature raking (*t*-test, KLD, CB).

FWHT-FSST		**PD vs. HC**			**HD vs. HC**			**ALS vs. HC**		
		ST	**EN**	**ALL**	**ST**	**EN**	**ALL**	**ST**	**EN**	**ALL**
Without feature ranking	AC	95.56	97.59	**97.56**	95	95.73	**97.23**	95.70	96.34	**96.97**
	SE	95.55	97.49	97.80	95.89	96.78	97.78	95.89	95.82	96.90
	SP	95.45	96.39	97.87	96.89	95.78	97.94	95	95.78	96.95
	PPV	95.45	97.30	97.46	95.45	96.76	97.21	95.67	95.15	97.80
	NPV	95.59	97.42	97.44	95.39	95.78	97.67	95.79	95.60	97.81
t-test	AC	97.37	99.08	**99.59**	97.76	99.87	**99.86**	97.67	97.63	**99.91**
	SE	97.30	99.21	99.97	97.86	99.68	99.78	97.63	97	99.05
	SP	97.39	97.90	99.4	97.78	99.73	99.65	97.46	97.19	99.85
	PPV	97.29	97.29	99.78	99.45	99.49	99.90	97.34	97.75	99.43
	NPV	97.28	99.56	99.42	97.29	99.38	99.76	97.29	97.43	99.54
KLD	AC	99.27	99	**99.52**	97.60	99.05	**99.90**	97.94	97.50	**100**
	SE	97.90	99.06	99.20	97.99	99.70	99.87	97.60	99.99	99.12
	SP	99.39	99.95	99.90	99.65	99.20	99.90	97.64	99.70	99.40
	PPV	99.40	99.05	99.90	99.76	99	99.87	97.59	99.78	99.51
	NPV	97.56	99.89	99.87	99.09	99.25	99.88	97.67	99.27	99.30
CB	AC	99.40	99.68	**100**	99.71	99.13	**100**	99.90	99.91	**100**
	SE	97.40	99	99.96	99.56	99.03	99.22	97.54	99.39	99.06
	SP	99.40	99.67	99.09	99.67	99.09	99.81	97.43	99.94	99.90
	PPV	99.30	99.57	99.90	99.45	99.45	99.70	97.03	99.60	99.41
	NPV	99.28	99.28	99.45	99.34	99.38	99.54	97.67	99.48	99.45

Classification performance of NDD using FWHT-FSST and feature raking (*t*-test, KLD, CB) is shown in **Table 7**. In a previous research study, wavelet transform was employed to detect gait abnormalities. Specifically, the Haar wavelet achieved a maximum classification accuracy of 90.32% for both right swing and left stance intervals and 100% accuracy for all left leg gait parameters combined. In the work of Joshi et al.[8], the distinctive characteristic of the Haar wavelet is its ability to emphasize sudden changes or discontinuities in data, making it well-suited for highlighting specific objects or patterns. This capacity to capture discontinuities, essential for efficient classification, is referred to as a transient phenomenon. In the current study, the higher classification accuracy achieved with the Haar wavelet suggests that one group's time series of gait variables exhibited abrupt changes compared to the other group. Additionally, the study compared different time series to elucidate their utility in assessing symmetry for detecting neurodegenerative diseases. Notably, the research introduced a novel classification method based on a sparse non-negative least squares (NNLS) coding strategy, which was employed for the first time to identify gait time intervals in patients with neurodegenerative diseases from those of healthy individuals.

Table 8 illustrates the classification accuracy of the proposed method compared to existing methods. Additionally, various classifier models were integrated into the classification task to enhance the detection of gait abnormalities.

Table 8. The comparative results of the proposed method and the existing method.

Proposed method	Classification task	Extracted Features	Classifier	Result
Topological Motion Analysis[50]	HC vs. PD	Stance, stride, swing intervals	Random Forest (RF)	AUC-0.9667
	HC vs. HD			0.9906
	HC vs. ALS			0.9135
Nonparametric Parzen-window[51]	HC vs. ALS	Frequency-based features	Support vector machine (SVM)	82.8% AUC-0.869
Topological Data Analysis[52]	HC vs. PD.	Topological features	Naive Bayes (NB), Decision tree, RF	90.32% with RF.
	HC vs. HD			94.44 with DT
	HC vs. ALS			86.21% with KNN
SVD[53]	HC vs. PD	Stride, swing intervals	K-Nearest Neighbor	96.3%
Radial basis function[54]	HC vs. PD	Minimum, maximum, average, standard deviation	SVM	89.33%
	HC vs. HD			90.28%
	HC vs. ALS			96.79%
	HC vs. NDD			92.87%
Mutual Information analysis[55]	HC vs. PD	Auto-correlation-based features, Data-driven features	DT	92.3%
	HC vs. HD			88.5%
	HC vs. ALS			96.2%
	HC vs. NDD			87.5%
Phase synchronization and conditional entropy[56]	HC vs. PD	Stance, swing, stride intervals	Principal component analysis	AUC-0.928
	HC vs. HD	Stance, swing, stride intervals		0.959
	HC vs. ALS			0.824
Proposed Method FHWT	HC vs. PD	Statistical and Entropy features (Minimum, Maximum, mean, STD, kurtosis, Skewness, NSTD, Energy, Log-energy, Shannon, Renyi, Tsallis)	ANN classifier	99.58
	HC vs. HD			99.95
	HC vs. ALS			100
Proposed Method FSST	HC vs. PD			99.76
	HC vs. HD			99.86
	HC vs. ALS			100
Proposed Method FWHT-FSST	HC vs. PD			100
	HC vs. HD			100
	HC vs. ALS			100

4. Conclusion

In this study, an effective method was developed for the early detection of neurodegenerative diseases. The remarkable level of accuracy achieved by this method demonstrates the effectiveness of the proposed approach. The framework was designed to distinguish between three neurodegenerative diseases (NDDs) by analyzing human gait time series data. This involved performing frequency (FWHT) and time-frequency (FSST) based analyses on the gait time series to break down the gait signals into coefficients. Statistical and Entropy features were then computed from these decomposed coefficients and ranked using feature ranking techniques. The most highly ranked optimal features were utilized with an ANN classifier, resulting in excellent classification performance across all experimental tasks, with maximum accuracies of 99.58% for PD vs. HC, 99.95% for HD vs. HC, and 100% for ALS vs. HC using FWHT. Similarly, using FSST, an accuracy of 99.76% for PD vs. HC, 99.86% for HD vs. HC, and 100% for ALS vs. HC was achieved. In our

future research activities, we plan to explore several aspects. Firstly, we intend to investigate how age, gender, and medication might impact the classification performance of our proposed tool. Additionally, we aim to expand upon our current work by incorporating various pattern recognition techniques and utilizing transformer architecture models. These enhancements will further enhance our classification performance's efficiency and effectiveness in future studies.

Author contributions

Conceptualization, JP, TG, MSPS and CP; methodology, JP and TG; software, MSPS and CP; validation, TG, MSPS and JP; formal analysis, JP, TG, MSPS and CP; investigation, CP; resources, CP; data curation, JP, TG, MSPS and CP; writing—original draft preparation, JP and TG; writing—review and editing, JP, TG JP and TG. All authors have read and agreed to the published version of the manuscript.

Data availability

The datasets generated during and/or analyzed during the current study are available at the https://www.physionet.org/content/gaitndd/1.0.0/.

Conflict of interest

The authors declare no conflict of interest.

References

1. Ren P, Tang S, Fang F, et al. Gait Rhythm Fluctuation Analysis for Neurodegenerative Diseases by Empirical Mode Decomposition. IEEE Transactions on Biomedical Engineering. 2017; 64(1): 52-60. doi: 10.1109/tbme.2016.2536438
2. Tysnes OB, Storstein A. Epidemiology of Parkinson's disease. Journal of Neural Transmission. 2017; 124(8): 901-905. doi: 10.1007/s00702-017-1686-y
3. Chiò A, Logroscino G, Traynor BJ, et al. Global Epidemiology of Amyotrophic Lateral Sclerosis: A Systematic Review of the Published Literature. Neuroepidemiology. 2013; 41(2): 118-130. doi: 10.1159/000351153
4. Suescun J, Chandra S, Schiess MC. The Role of Neuroinflammation in Neurodegenerative Disorders. In: Translational inflammation. Academic Press; 2019. pp. 241-267.
5. Dharmadasa T, Matamala JM, Huynh W, et al.Motor neurone disease. In: Handbook of clinical neurology. pp. 345-357.
6. Golbe LI, Mark MH, Sage J. Parkinson's disease handbook. American Parkinson Disease Association; 2009.
7. Reilmann R. Parkinsonism in Huntington's disease. International Review of Neurobiology. 2019; 149: 299-306. doi: 10.1016/bs.irn.2019.10.006
8. Joshi D, Khajuria A, Joshi P. An automatic non-invasive method for Parkinson's disease classification. Computer Methods and Programs in Biomedicine. 2017; 145: 135-145. doi: 10.1016/j.cmpb.2017.04.007
9. El-Alfy H, Mitsugami I, Yagi Y. Gait Recognition Based on Normal Distance Maps. IEEE Transactions on Cybernetics. 2018; 48(5): 1526-1539. doi: 10.1109/tcyb.2017.2705799
10. Xia Y, Gao Q, Ye Q. Classification of gait rhythm signals between patients with neuro-degenerative diseases and normal subjects: Experiments with statistical features and different classification models. Biomedical Signal Processing and Control. 2015; 18: 254-262. doi: 10.1016/j.bspc.2015.02.002
11. Zeng W, Wang C. Classification of neurodegenerative diseases using gait dynamics via deterministic learning. Information Sciences. 2015; 317: 246-258. doi: 10.1016/j.ins.2015.04.047
12. Poria S, Hazarika D, Majumder N, et al. Meld: A multimodal multi-party dataset for emotion recognition in conversations. arXiv:1810.02508. 2018.
13. Rovini E, Maremmani C, Cavallo F. How Wearable Sensors Can Support Parkinson's Disease Diagnosis and Treatment: A Systematic Review. Frontiers in Neuroscience. 2017; 11. doi: 10.3389/fnins.2017.00555
14. Beyrami SMG, Ghaderyan P. A robust, cost-effective and non-invasive computer-aided method for diagnosis three types of neurodegenerative diseases with gait signal analysis. Measurement. 2020; 156: 107579. doi: 10.1016/j.measurement.2020.107579
15. Soubra R, Diab MO, Moslem B. Identification of Parkinson's disease by using multichannel Vertical Ground Reaction Force signals. In: Proceedings of the 2016 International Conference on Bio-engineering for Smart Technologies (BioSMART). IEEE. pp. 1-4.
16. Wu Y, Chen P, Luo X, et al. Measuring signal fluctuations in gait rhythm time series of patients with Parkinson's disease using entropy parameters. Biomedical Signal Processing and Control. 2017; 31: 265-271. doi:

10.1016/j.bspc.2016.08.022
17. Schalkamp AK, Peall KJ, Harrison NA, Sandor C. Wearable movement-tracking data identify Parkinson's disease years before clinical diagnosis. Nature Medicine. 2023; 29(8): 2048-2056. doi.org/10.1038/s41591-023-02440-2
18. Liu AB, Lin CW. Multiscale Approximate Entropy for Gait Analysis in Patients with Neurodegenerative Diseases. Entropy. 2019; 21(10): 934. doi: 10.3390/e21100934
19. Yu J, Cao J, Liao WH, et al. Multivariate Multiscale Symbolic Entropy Analysis of Human Gait Signals. Entropy. 2017; 19(10): 557. doi: 10.3390/e19100557
20. Liao F, Wang J, He P. Multi-resolution entropy analysis of gait symmetry in neurological degenerative diseases and amyotrophic lateral sclerosis. Medical Engineering & Physics. 2008; 30(3): 299-310. doi: 10.1016/j.medengphy.2007.04.014
21. Mengarelli A, Tigrini A, Fioretti S, et al. Identification of Neurodegenerative Diseases from Gait Rhythm Through Time Domain and Time-Dependent Spectral Descriptors. IEEE Journal of Biomedical and Health Informatics. 2022; 26(12): 5974-5982. doi: 10.1109/jbhi.2022.3205058
22. Setiawan F, Lin CW. Identification of Neurodegenerative Diseases Based on Vertical Ground Reaction Force Classification Using Time–Frequency Spectrogram and Deep Learning Neural Network Features. Brain Sciences. 2021; 11(7): 902. doi: 10.3390/ brainsci11070902
23. Warule P, Mishra SP, Deb S. Time-frequency analysis of speech signal using Chirplet transform for automatic diagnosis of Parkinson's disease. Biomedical Engineering Letters. 2023; 13(4): 613-623. doi: 10.1007/s13534-023-00283-x
24. Setiawan F, Liu AB, Lin CW. Development of Neuro-Degenerative Diseases' Gait Classification Algorithm Using Convolutional Neural Network and Wavelet Coherence Spectrogram of Gait Synchronization. IEEE Access. 2022; 10: 38137-38153. doi: 10.1109/access.2022.3158961
25. Prasanna J, Subathra MSP, Mohammed MA, et al. Detection of Focal and Non-Focal Electroencephalogram Signals Using Fast Walsh-Hadamard Transform and Artificial Neural Network. Sensors. 2020; 20(17): 4952. doi: 10.3390/s20174952
26. Saka K, Aydemir O, Ozturk M. Classification of EEG Signals Recorded During Right/Left Hand Movement Imagery Using Fast Walsh Hadamard Transform Based Features. In: Proceedings of the 2016 39th International Conference on Telecommunications and Signal Processing (TSP); 27–29 June 2016; Vienna, Austria. pp. 413-416.
27. Sareen S, Sood SK, Gupta SK. A Cloud-Based Seizure Alert System for Epileptic Patients That Uses Higher-Order Statistics. Computing in Science & Engineering. 2016; 18(5): 56-67. doi: 10.1109/mcse.2016.82
28. Amira A, Bouridance A, Milligan P, et al. Novel FPGA implementations of Walsh-Hadamard transforms for signal processing. IEEE Proc. Image Signal Process. 2001; 148: 377-383.
29. Deveci TC, Cakir S. Cetin AE. Energy Efficient Hadamard Neural Networks. arXiv:1805.05421. 2018; 1-15.
30. Oberlin T, Meignen S, Perrier V. The Fourier-based synchrosqueezing transform. In: Proceedings of the 2014 IEEE international conference on acoustics, speech and signal processing (ICASSP). pp. 315-319.
31. Gundewar SK, Kane PV. Bearing fault diagnosis using time segmented Fourier synchrosqueezed transform images and convolution neural network. Measurement. 2022; 203: 111855. doi: 10.1016/j.measurement.2022.111855
32. Mamli S, Kalbkhani H. Gray-level co-occurrence matrix of Fourier synchro-squeezed transform for epileptic seizure detection. Biocybernetics and Biomedical Engineering. 2019; 39(1): 87-99. doi: 10.1016/j.bbe.2018.10.006
33. Li L, Cai H, Han H, et al. Adaptive short-time Fourier transform and synchrosqueezing transform for non-stationary signal separation. Signal Processing. 2020; 166: 107231. doi: 10.1016/j.sigpro.2019.07.024
34. Daliri MR. Automatic diagnosis of neuro-degenerative diseases using gait dynamics. Measurement. 2012; 45(7): 1729-1734. doi: 10.1016/j.measurement.2012.04.013
35. Acharya UR, Fujita H, Sudarshan VK, et al. Application of entropies for automated diagnosis of epilepsy using EEG signals: A review. Knowledge-Based Systems. 2015; 88: 85-96. doi: 10.1016/j.knosys.2015.08.004
36. Lemons DS, Lemons DS. A student's guide to Entropy. Cambridge university press; 2013.
37. Renyi A. On measures of Entropy and information, Berkeley Symp. On Math. Statist. And Prob. 1961; 1: 547-561.
38. Cachin C. Smooth entropy and Renyi entropy, Advances in Cryptology Eurocrypt. Springer, Berlin Heidelberg; 2001. pp. 193-208.
39. Bezerianos A, Tong S, Thakor N. Time-Dependent Entropy Estimation of EEG Rhythm Changes Following Brain Ischemia. Annals of Biomedical Engineering. 2003; 31(2): 221-232. doi: 10.1114/1.1541013
40. Tong S, Bezerianos A, Malhotra A, et al. Parameterized entropy analysis of EEG following hypoxic-ischemic brain injury. Phys. Lett. A. 2003; 314(5-6): 354-361.
41. Geng X, Liu TY, Qin T, et al. Feature selection for ranking. In: Proceedings of the 30th annual international ACM SIGIR conference on research and development in information retrieval. pp. 407-414.
42. Shri TP, Sriraam N. Comparison of t-test ranking with PCA and SEPCOR feature selection for wake and stage 1 sleep pattern recognition in multichannel electroencephalograms. Biomedical Signal Processing and Control. 2017; 31: 499-512.
43. Ponti M, Kittler J, Riva M, et al. A decision cognizant Kullback–Leibler divergence. Pattern Recognition. 2017; 61: 470-478. doi: 10.1016/j.patcog.2016.08.018
44. Mookiah MRK, Chua CK, Min LC, et al. Computer Aided Diagnosis of Diabetic Retinopathy Using Multi-Resolution Analysis and Feature Ranking Frame Work. Journal of Medical Imaging and Health Informatics. 2013;

3(4): 598-606. doi: 10.1166/jmihi.2013.1210
45. Mookiah MRK, Acharya UR, Koh JEW, et al. Decision support system for age-related macular degeneration using discrete wavelet transform. Medical & Biological Engineering & Computing. 2014; 52(9): 781-796. doi: 10.1007/s11517-014-1180-8
46. Kumar R, Singh B, Shahani DT, et al. Recognition of Power-Quality Disturbances Using S-Transform-Based ANN Classifier and Rule-Based Decision Tree. IEEE Transactions on Industry Applications. 2015; 51(2): 1249-1258. doi: 10.1109/tia.2014.2356639
47. Rai HM, Trivedi A, Shukla S. ECG signal processing for abnormalities detection using multi-resolution wavelet transform and Artificial Neural Network classifier. Measurement. 2013; 46(9): 3238-3246. doi: 10.1016/j.measurement.2013.05.021
48. Ranganathan A. The levenberg-marquardt algorithm. Tutoral on LM algorithm. 2004; 11(1): 101-110.
49. Ghaderyan P, Beyrami SMG. Neurodegenerative diseases detection using distance metrics and sparse coding: A new perspective on gait symmetric features. Computers in Biology and Medicine. 2020; 120: 103736. doi: 10.1016/j.compbiomed.2020.103736
50. Yan Y, Omisore OM, Xue YC, et al. Classification of Neurodegenerative Diseases via Topological Motion Analysis—A Comparison Study for Multiple Gait Fluctuations. IEEE Access. 2020; 8: 96363-96377. doi: 10.1109/access.2020.2996667
51. Wu Y, Shi L. Analysis of altered gait cycle duration in amyotrophic lateral sclerosis based on nonparametric probability density function estimation. Medical Engineering & Physics. 2011; 33(3): 347-355. doi: 10.1016/j.medengphy.2010.10.023
52. Yan Y, Ivanov K, Mumini Omisore O, et al. Gait Rhythm Dynamics for Neuro-Degenerative Disease Classification via Persistence Landscape- Based Topological Representation. Sensors. 2020; 20(7): 2006. doi: 10.3390/s20072006
53. Tuncer T, Dogan S, Acharya UR. Automated detection of Parkinson's disease using minimum average maximum tree and singular value decomposition method with vowels. Biocybernetics and Biomedical Engineering. 2020; 40(1): 211-220. doi: 10.1016/j.bbe.2019.05.006
54. Gupta K, Khajuria A, Chatterjee N, et al. Rule based classification of neurodegenerative diseases using data driven gait features. Health and Technology. 2018; 9(4): 547-560. doi: 10.1007/s12553-018-0274-y
55. Ren P, Zhao W, Zhao Z, et al. Analysis of Gait Rhythm Fluctuations for Neurodegenerative Diseases by Phase Synchronization and Conditional Entropy. IEEE Transactions on Neural Systems and Rehabilitation Engineering. 2016; 24(2): 291-299. doi: 10.1109/tnsre.2015.2477325
56. Marin-Lopez A, Martinez-Martinez F, Martínez-Cadena JA, et al. Multiscale SVD entropy for the analysis of gait dynamics. Biomedical Signal Processing and Control. 2024; 87: 105439. doi: 10.1016/j.bspc.2023.105439